

**Balancing Act: Evidence for a Strong Subdominant  $d$ -Wave Pairing Channel in  $\text{Ba}_{0.6}\text{K}_{0.4}\text{Fe}_2\text{As}_2$** T. Böhm,<sup>1,2,3</sup> A. F. Kemper,<sup>4</sup> B. Moritz,<sup>3</sup> F. Kretzschmar,<sup>1,2</sup> B. Muschler,<sup>1,2,†</sup> H.-M. Eiter,<sup>1,2</sup> R. Hackl,<sup>1,\*</sup>  
T. P. Devereaux,<sup>3,5</sup> D. J. Scalapino,<sup>6</sup> and Hai-Hu Wen<sup>7</sup><sup>1</sup>Walther Meissner Institut, Bayerische Akademie der Wissenschaften, 85748 Garching, Germany<sup>2</sup>Physik-Department E23, Technische Universität München, 85748 Garching, Germany<sup>3</sup>Stanford Institute for Materials and Energy Sciences, SLAC National Accelerator Laboratory,  
2575 Sand Hill Road, Menlo Park, California 94025, USA<sup>4</sup>Lawrence Berkeley National Laboratory, 1 Cyclotron Road, Berkeley, California 94720, USA<sup>5</sup>Geballe Laboratory for Advanced Materials and Department of Applied Physics,  
Stanford University, California 94305, USA<sup>6</sup>Physics Department, University of California, Santa Barbara, California 93106-9530, USA<sup>7</sup>National Laboratory of Solid State Microstructures and Department of Physics,  
Nanjing University, Nanjing 210093, China

(Received 18 August 2014; published 18 December 2014)

We present detailed measurements of the temperature-dependent Raman spectra of optimally doped  $\text{Ba}_{0.6}\text{K}_{0.4}\text{Fe}_2\text{As}_2$  and analyze the low-temperature spectra based on local-density-approximation band-structure calculations and the subsequent estimation of effective Raman vertices. Experimentally, a narrow, emergent mode appears in the  $B_{1g}$  ( $d_{x^2-y^2}$ ) Raman spectra only below  $T_c$ , well into the superconducting state and at an energy below twice the energy gap on the electron Fermi-surface sheets. The Raman spectra can be reproduced quantitatively with estimates for the magnitude and momentum-space structure of an  $A_{1g}$  ( $s$ -wave) pairing gap on different Fermi-surface sheets, as well as the identification of the emergent sharp feature as a Bardasis-Schrieffer exciton. Formed as a Cooper-pair bound state in a subdominant  $d_{x^2-y^2}$  channel, the binding energy of the exciton relative to the gap edge shows that the coupling strength in the subdominant channel is as strong as 60% of that in the dominant  $s$ -wave channel. This result suggests that  $d_{x^2-y^2}$  may be the dominant pairing symmetry in Fe-based superconductors that lack central hole bands.

DOI: 10.1103/PhysRevX.4.041046

Subject Areas: Condensed Matter Physics,  
Superconductivity**I. INTRODUCTION**

Superconductivity appears in close proximity to magnetically ordered phases in iron-based superconductors (FeSCs) [1–3]; however, as inherently multiband materials, the topology of the Fermi surface plays an especially important role in determining the ordered state [4,5]. This sensitivity was demonstrated explicitly for single-layer FeSe [6], which may become superconducting already above 60 K possibly due to the interplay of intraband and interband Cooper pairing [7]. In FeSCs, the structure, size, and, potentially, symmetry of the gap function  $\Delta_{\mathbf{k}}$  are expected to react sensitively to small changes in external control parameters such as doping or pressure [8–12]. Additionally, the symmetry of  $\Delta_{\mathbf{k}}$  reflects

the dominant channel for Cooper pairing and allows insight into unconventional pairing mechanisms driven by band-structure-dependent electronic interactions. Finding the proper experimental tools to monitor changes of the pairing state may provide a possible pathway for a quantitative description of superconductivity in the FeSCs.

One of the hallmarks of superconductivity in  $\text{Ba}_{0.6}\text{K}_{0.4}\text{Fe}_2\text{As}_2$  is the observation of the neutron resonance [13] which favors the  $s_{+-}$  state predicted by Mazin and co-workers [1] but still leaves space for an  $s_{++}$  state driven by orbital fluctuations [14]. In either case, the nesting between the central hole bands and the electron bands takes advantage of strong interactions at short distances corresponding to large momentum transfers of  $(\pi, 0)$  (in the 1 Fe unit cell). Similarly, the electron bands themselves can gain from the  $(\pi, \pi)$  scattering of nearly equal strength [2,3,15,16]. Hence, two unconventional pairing states  $s_{+-}$  (higher-order  $A_{1g}$ ) and  $d_{x^2-y^2}$  (lowest-order  $B_{1g}$ ) resulting from  $(\pi, 0)$  and  $(\pi, \pi)$  scattering, respectively, can be expected to compete and may be tuned by intentionally changing the band structure.

The close proximity of these pairing instabilities leaves spectroscopic fingerprints. In the single-particle spectra,

\*Corresponding author.

Hackl@wmi.badw.de

†Present address: Zoller &amp; Fröhlich GmbH, Simoniusstrasse 22, 88239 Wangen im Allgäu, Germany.

Published by the American Physical Society under the terms of the Creative Commons Attribution 3.0 License. Further distribution of this work must maintain attribution to the author(s) and the published article's title, journal citation, and DOI.

one expects characteristic momentum dependence of the gaps on the Fermi surfaces of multiband systems. If the gap changes sign between different sheets of the Fermi surface, the quasiparticle interference observed in tunneling spectra may demonstrate the influence from applied magnetic fields [17]. In a light-scattering experiment, new or emergent collective modes are expected in addition to the more familiar pair-breaking peak at an energy twice the gap maximum [18]. Generally, these collective modes can appear in the particle-hole or particle-particle channel either separately or together ( $\tau_3$  or  $\tau_2$  channels, respectively, in the language of Nambu). A critical question is which of these modes can be visible in Raman-scattering measurements and which conclusions can be derived from their energies and symmetries. We briefly outline the possibilities.

In multiband systems including FeSCs, the (weakly) coupled densities of the superconducting condensates on the individual bands can beat against each other, and Josephson-like excitations are expected, as discussed first by Leggett [19]. The absolute energy of these modes scales with the interband coupling strength [20]. Although there exist no systematic studies on Leggett modes, the data on MgB<sub>2</sub> suggest that one of the Raman-active modes in the energy range below the gap may originate from a weak coupling between the two-dimensional (2D)  $\sigma$  band which possesses a large gap and the more 3D  $\pi$  band [20,21].

A second possibility is modes associated with coupled amplitude fluctuations of superconducting and density-wave gaps, which was extensively studied in charge-density-wave (CDW) systems [22–27]. The coupling between the condensates allows a  $\tau_2$  collective amplitude mode (analogous to the Higgs boson) to be visible in Raman-scattering measurements in addition to the  $\tau_3$  CDW amplitude mode alone and to reflect the coupling strength [28]. In both NbSe<sub>2</sub> and the A15 compounds V<sub>3</sub>Si and Nb<sub>3</sub>Sn, resolution-limited lines below twice the gap edge have been observed [22,29]. Evidence for amplitude modes in these compounds was derived from the approximate conservation of the integrated spectral weight either as a function of applied field [22] or temperature [23,29–31]. However, while the existence of a CDW is well established in NbSe<sub>2</sub>, there is no evidence of CDW order in A15 compounds at lower temperatures. Yet, structural transformations from a high-temperature-cubic to a low-temperature-tetragonal lattice occur above the superconducting transition temperature [32]. Similar to the case of the amplitude mode in NbSe<sub>2</sub>, spectral weight is transferred into the collective mode from the strongly coupled phonon that drives the transition.

The conceptual complication encountered in the case of the A15 compounds V<sub>3</sub>Si and Nb<sub>3</sub>Sn triggered an alternative explanation of the in-gap modes in terms of exciton-like bound states [33]. They can originate from residual interactions between the electrons of a broken Cooper pair [33–36] in close analogy to excitons in semiconductors.

First predicted by Bardasis and Schrieffer (BS) [33–35], excitonic or electron-pair bound states can be formed, depending on the sign of the residual interaction. These modes may exist as sharp features below the gap in *s*-wave superconductors or they may be damped considerably due to the existence of quasiparticles below the gap maximum in the presence of gap nodes in *d*-wave superconductors [37]. The energy difference between these modes and the gap edge reflects the relative strength of the residual interaction with respect to the binding energy of the ground state.

BS modes have been observed in superfluid <sup>4</sup>He (Ref. [38]), where they correspond to bound pairs of rotons, and explain the discrepancies between neutron- and light-scattering spectra [39]. However, they remain elusive in superconductors, requiring a sufficiently strong subdominant interaction to be clearly distinguishable. Recently, narrow in-gap modes were observed by Raman measurements on Ba<sub>0.6</sub>K<sub>0.4</sub>Fe<sub>2</sub>As<sub>2</sub> and interpreted in terms of BS modes [40]. In this case, the intensity does not come from a phonon, some of which gain rather than lose spectral weight upon entering the superconducting state, but is drained from the pair-breaking peaks. This experimental observation is qualitatively different from what was found in previous studies of A15 compounds [18], but the effect was predicted specifically for the iron-based compounds with competing *s*- and *d*-wave pairing states [41–43]. Therefore, the earlier qualitative argumentation [40] needs to be augmented both experimentally and theoretically.

In this work, we present experimental polarization-dependent Raman spectra for various temperatures between 8 and 46 K and perform weak-coupling calculations for the  $T = 0$  Raman response for a realistic band structure, taking into account interactions between the five bands close to the Fermi level. The observation and theoretical analysis of an emergent mode at 140 cm<sup>-1</sup>, being well separated from the other pair-breaking peaks, appearing only in  $B_{1g}$  symmetry, stealing spectral weight only from electronic features, and exhibiting a BCS-like temperature dependence, allows us to unambiguously identify it as a  $d_{x^2-y^2}$  BS exciton. From the energy position and the spectral weight of the exciton, we estimate the relative strength of the subdominant  $d_{x^2-y^2}$  pairing channel to be more than half as strong as the dominant  $s_{+-}$  channel. Our results suggest that the  $d_{x^2-y^2}$  pairing channel may indeed become dominant when the  $s_{+-}$  interaction is reduced, for example, by the absence of hole pockets at the center of the Brillouin zone.

## II. EXPERIMENTAL STUDY OF THE TEMPERATURE DEPENDENCE

In Ba<sub>0.6</sub>K<sub>0.4</sub>Fe<sub>2</sub>As<sub>2</sub>, superconductivity-induced features were found in  $A_{1g}$ ,  $B_{1g}$ , and  $B_{2g}$  symmetry experimentally accessible with light polarizations in the Fe planes [40]. Although the crystal unit cell involves two Fe atoms per unit cell due to the staggered positioning of the As above

and below the Fe planes, it is convenient instead to make a group-theory reference in the 1 Fe unit cell where polarizations and selection rules can be framed in terms of polarizations along the Fe-Fe bond direction. In the  $B_{1g}$  spectra (1 Fe unit cell), the observation of very narrow modes at low temperature suggests the existence of collective excitations and their interpretation in terms of excitonic BS modes. However, the temperature dependence of the energy and the emergence of this mode require further study.

Before describing the quantitative theoretical analysis in the zero-temperature limit, we present an additional set of experiments in the range  $8 \text{ K} \leq T \leq 46 \text{ K}$ , since, somewhat counterintuitively, the in-gap modes and the usual pair-breaking features are expected to depend differently on temperature in systems with elastic or inelastic quasiparticle scattering [44–46]. In either case, the variation of the pair-breaking maxima  $\Omega_{\text{PB}}(T)$  in the Raman spectra is determined by the temperature dependence of both the gap  $\Delta(T)$  and the quasiparticle relaxation rate  $\Gamma(T)$  resulting from scattering. The interplay of  $\Delta(T)$  and  $\Gamma(T)$  in the Raman response can make the temperature dependence of  $\Omega_{\text{PB}}(T)$  deviate substantially from that of  $\Delta(T)$  [44–46]. On the other hand, the energy  $\Omega_{\text{BS}}(T)$  of the  $\delta$ -like BS modes is directly proportional to the single-particle gap  $\Delta(T)$  modulo a weakly temperature- and energy-dependent coupling constant [33,39]. Since  $\Delta(T)$  has been measured independently and found to follow the BCS prediction [47],  $\Omega_{\text{BS}}(T)$  is better defined than  $\Omega_{\text{PB}}(T)$  and one can hope to observe a difference in the temperature dependences.

Experiments are performed on a freshly cleaved surface of the same optimally hole-doped single crystal of  $\text{Ba}_{0.6}\text{K}_{0.4}\text{Fe}_2\text{As}_2$  that has been used in previous studies and possesses a superconducting transition at  $T_c = 38.5 \text{ K}$  (Ref. [40]). We use an Ar ion laser emitting at 514 nm and a standard scanning spectrometer with the sample held in a cryogenically pumped vacuum. We measure spectra with linear polarizations of the incoming and outgoing photons oriented perpendicular and at  $45^\circ$  with respect to the Fe-Fe direction ( $0^\circ$  with respect to the crystallographic axes) to project the  $B_{1g}$  and  $A_{2g}$  symmetries. No subtraction procedure is applied, as the  $A_{2g}$  component is found to be weak [48,49]. The  $B_{1g}$  spectra contain all relevant features for this analysis of the temperature dependence.

The spectra measured at various temperatures between 8 and 46 K are shown in Fig. 1(a). At low temperature, one observes two prominent peaks at 140 and 170  $\text{cm}^{-1}$  and a weak one at 70  $\text{cm}^{-1}$ , which were all previously identified with collective modes [40]. The mode at 140  $\text{cm}^{-1}$  has the smallest low-temperature width. Following the positions of the three peaks [dashed vertical lines in Fig. 1(a) show the low-temperature limit] indicates distinct differences, with the mode at 140  $\text{cm}^{-1}$  (filled circle) displaying the strongest shift and the peaks at 70  $\text{cm}^{-1}$  and the gap edge at 170  $\text{cm}^{-1}$  (open circle) varying only weakly. The positions

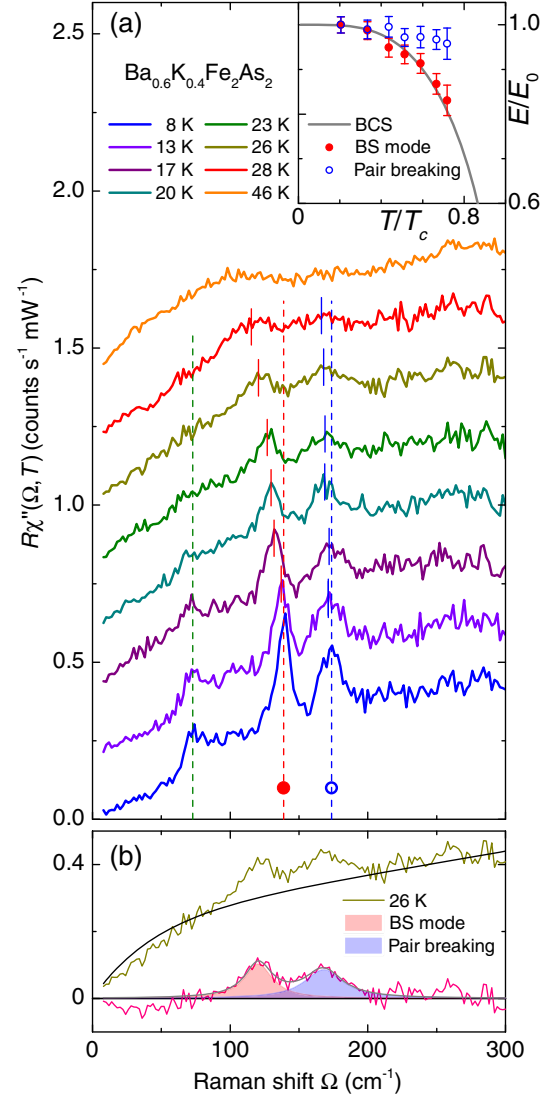


FIG. 1. Temperature dependence of the Raman spectra of  $\text{Ba}_{0.6}\text{K}_{0.4}\text{Fe}_2\text{As}_2$  in  $B_{1g}$  symmetry. (a) The spectra measured above 8 K are consecutively shifted up by 0.2 units. The pair-breaking features (open symbols) and the collective mode (full circles) depend differently on temperature, as shown in the inset (having a suppressed energy of 0). The pair-breaking maximum exhibits a temperature dependence that is different from BCS due to interaction effects [45,46]. (b) The peak energies are determined by fitting the spectra with two Lorentzians and a smooth phenomenological background (black curve).

are determined following a phenomenological background [50] subtraction [Fig. 1(b)]. In the inset of Fig. 1(a), the positions of the two high-energy peaks relative to their low-temperature limiting values are shown along with the BCS prediction for the energy gap. Only the mode at 140  $\text{cm}^{-1}$  is close to the mean-field expectation in striking similarity with the single-particle gaps [47], making it a likely candidate for a BS exciton. With increasing temperature, the width of the line increases due to quasiparticle damping, making it indiscernible at sample temperatures above 28 K.

The additional experimental observations shown here facilitate a clear distinction between the various spectral features and motivate us to explain the modes at 70 and 170  $\text{cm}^{-1}$  in terms of pair breaking and identify only the line at 140  $\text{cm}^{-1}$  with a BS exciton, considerably simplifying the theoretical analysis. Nevertheless, it remains crucially important to work with a realistic band structure, since the vertex corrections result from interband terms [41] rather than from intraband anisotropies of the interaction potential  $V_{\mathbf{k},\mathbf{k}'}$  as derived first by Bardasis and Schrieffer [34] and discussed in detail later in the context of light scattering [33,35].

### III. MODEL DESCRIPTION

The model employed here is based on a realistic tight-binding band structure derived from density-functional-theory estimates using the local density approximation [16] and the analysis of final-state interactions to provide a semiquantitative theoretical description of the Raman spectra for optimally hole-doped  $\text{Ba}_{0.6}\text{K}_{0.4}\text{Fe}_2\text{As}_2$  in the zero-temperature limit. A full description of the temperature dependence of the entire spectra in the superconducting state would require the knowledge of all relevant interactions and a strong-coupling Eliashberg calculation. Since the understanding of the dynamical interactions in the FeSC is still incomplete, we limit the quantitative analysis to zero temperature and argue only qualitatively in the case of finite temperatures.

The band structure  $E_n(\mathbf{k})$ , where  $n$  is the band index, is generated from a tight-binding approximation to the local-density-approximation bands, including all five Fe  $d$  orbitals developed by Graser *et al.* [16] for undoped  $\text{BaFe}_2\text{As}_2$ . For  $\text{Ba}_{0.6}\text{K}_{0.4}\text{Fe}_2\text{As}_2$ , the Fermi energy is shifted down by 144 meV with respect to the original band structure to account for the substitution of 40% Ba by K, which adds 0.2 holes per Fe atom and reduces the filling to 5.8. Transforming the system from an orbital basis to a band basis gives five bands, of which four cross the Fermi level, including the two hole bands at the Brillouin-zone (BZ) center, one hole band at the  $M$  point, and an electron band encircling the  $X$  point. The presence of the 2 Fe unit cell requires a backfolding of the 1 Fe BZ, achieved by adding another five bands, shifted by  $\mathbf{k} = (\pi, \pi, \pi)$ , to the existing ones. This vector accounts for the additional translational symmetry of the 2 Fe BZ. Five of the resulting ten bands cross the Fermi level: three hole bands at the BZ center ( $h1$ ,  $h2$ , and  $h3$  from the inside out) and two electron bands around the  $X$  point ( $e1$  and  $e2$  from the outside in). The Fermi surfaces of the hole bands intersect each other on lines, as do the electron bands. Since the intersecting bands derive from the same orbitals, the degeneracies are lifted [52] by any small residual interaction. (We use 25 meV for all bands and show in Appendix B that the hybridization energy influences the Raman spectra only weakly.)

The momentum-dependent vertices (form factors)  $\gamma_n^\mu$  ( $\mu = A_{1g}, B_{1g}, B_{2g}$ ) for band  $n$  determine the symmetry-dependent sensitivity of the experiment in  $k$  space [18,53]. The form factors can be determined either on the basis of symmetry arguments [18,39,48,53,54], via the full scattering process [55], or by exploiting the curvature of the conduction bands being inversely proportional to the second derivative of the band structure (effective-mass approximation). In the limit of vanishing photon energies, the latter two approaches are equivalent [18,56]. The effective-mass approximation is justified here [52] since the incident photons have energies lower than resonance energies. The related vertices  $\gamma_n^\mu$  are derived numerically at the Fermi energy  $E_F$  from the dispersion  $E_n(\mathbf{k})$  for each band and are given by

$$\gamma_n^{A_{1g}}(\mathbf{k}) = \frac{1}{2} \left\{ \frac{\partial^2 E_n(\mathbf{k})}{\partial k_x \partial k_x} + \frac{\partial^2 E_n(\mathbf{k})}{\partial k_y \partial k_y} \right\}, \quad (1)$$

$$\gamma_n^{B_{1g}}(\mathbf{k}) = \frac{1}{2} \left\{ \frac{\partial^2 E_n(\mathbf{k})}{\partial k_x \partial k_x} - \frac{\partial^2 E_n(\mathbf{k})}{\partial k_y \partial k_y} \right\}, \quad (2)$$

$$\gamma_n^{B_{2g}}(\mathbf{k}) = \frac{\partial^2 E_n(\mathbf{k})}{\partial k_x \partial k_y} \quad (3)$$

and shown in Fig. 2. Here,  $k_{x,y}$  refer to momenta along Fe-Fe bond directions. Although the bands are calculated for the 2 Fe BZ, we continue to use the 1 Fe BZ reference frame because the experiments clearly show that the symmetry selection rules are dominated by the 1 Fe cell [40,48,57]. Additionally, in the 2 Fe BZ cell, the role of the  $B_{1g}$  and  $B_{2g}$  projections would be interchanged in a counterintuitive way such that the  $d_{x^2-y^2}$  type of interaction between the electron bands would appear in the  $B_{2g}$  (or  $xy$ ) channel. In fact, the 1 Fe BZ captures most of the features and simplifies the argumentation considerably, while for the 2 Fe BZ, improvements are found only on a quantitative level while the results are qualitatively similar [48].

Figures 2(b) and 2(c) show directly that the strongest contributions for the  $B_{1g}$  and  $B_{2g}$  spectra come from the outer electron band. For a more quantitative statement, the contribution from superconductivity to the Raman response  $\chi''(\mathbf{q} = 0, \Omega) = \text{Im}\chi(\mathbf{q} = 0, \Omega)$  is evaluated by an intraband bare-bubble approximation

$$\chi(\Omega) = \sum_n \sum_{\mathbf{k}} \gamma_n^2(\mathbf{k}) \lambda_n(\mathbf{k}, \Omega), \quad (4)$$

where the  $\lambda_n(\mathbf{k}, \Omega)$  is given by the Tsuneto function [58], where  $\Omega$  is the Raman shift. Neglecting band-structure effects, the expression for the response at  $T = 0$  can be transformed into

$$\chi''(\Omega) = 4\pi \sum_n \left\langle \frac{\gamma_n^2(\mathbf{k}) |2\Delta_n(\mathbf{k})|^2}{\Omega \sqrt{\Omega^2 - |2\Delta_n(\mathbf{k})|^2}} \right\rangle, \quad (5)$$

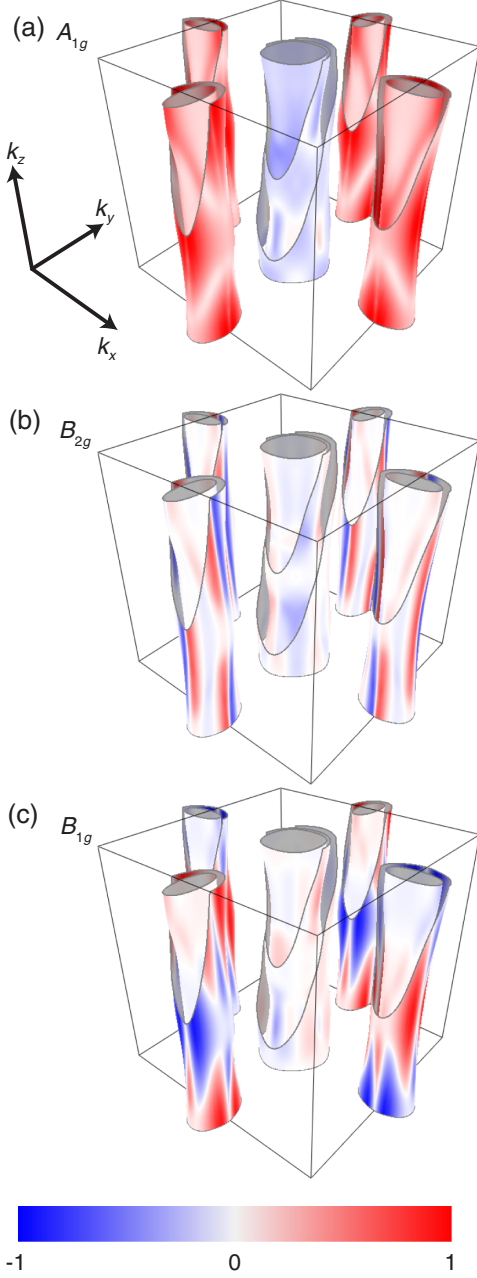


FIG. 2. Raman vertices in (a)  $A_{1g}$ , (b)  $B_{2g}$ , and (c)  $B_{1g}$  symmetry at the Fermi energy  $E_F$ . The black frame represents the 1 Fe BZ ranging from  $-\pi$  to  $\pi$  in each dimension  $k_x$ ,  $k_y$ , and  $k_z$ . There are three Fermi surfaces in the center and two at each face (the outer ones are cut open to visualize the inner ones) showing the hole bands and electron bands, respectively. All three symmetries have a common color scale that shows the sign and intensity of the Raman vertex at the Fermi surface. The hole bands around the BZ edges are equivalent to those in the center and are omitted for simplicity.

where  $\Omega > |2\Delta_n(\mathbf{k})|$  and the angled brackets denote an average over the Fermi-surface sheet  $n$ . The only relevant physical parameters that are varied to achieve the best agreement with the data are  $\mathbf{k}$ -dependent gap structures  $\Delta_n(\mathbf{k})$  for each Fermi surface. In addition, the relative

intensities of the spectra are scaled by 0.3, 0.6, and 1 for  $A_{1g}$ ,  $B_{1g}$ , and  $B_{2g}$ , respectively. For the  $A_{1g}$  spectra, Coulomb screening has to be included [59], but the effects are found to be very small since the gaps on the electron and hole bands are quite symmetric (except for the outer hole band), and the concomitant sign change of the Raman vertex nearly cancels all the screening contributions [41,52,59,60].

In addition to the lowest-order response (bare bubble) described by Eq. (5), vertex corrections will be considered for possibly explaining the bound state inside the gap along with the superconducting pair-breaking features. They make the theory gauge invariant [34] and describe the final-state interaction between the two electrons of a Cooper pair that has been broken by a photon [33,35]. The dynamics of bound states becomes important whenever the pairing potential is anisotropic [34], bringing interactions beyond ground-state Cooper pairing into play. This effect is important in the FeSCs having multiple bands at high-symmetry points. The full model is gauge invariant and accounts for both the pair-breaking effect and the final-state interaction on a realistic 3D multiband tight-binding band structure.

Here, contributions originating from a  $d$ -wave attractive coupling between the outer electron bands will be included that lead to a collective excitonic mode in  $B_{1g}$  symmetry [41]. The additional coupling  $g(\mathbf{k})$  contributes to the anisotropy of  $V_{\mathbf{k},\mathbf{k}'}$  and is assumed to be relevant only between the outer electron bands ( $e1$  in Table I). The influence of the interactions has been found to be negligible on the response from  $e2$ . We further assume that  $V_{\mathbf{k},\mathbf{k}'}$  is separable and varies as  $g(\mathbf{k})\lambda_d g(\mathbf{k}')$  with  $g(\mathbf{k})$  proportional to  $\gamma^{B_{1g}}(\mathbf{k})$  and normalized in a way that  $\lambda_d$  measures the strength of the  $d$ -wave interaction.  $g(\mathbf{k})$  causes multiple scattering processes and leads to an additive term in the response of the outer electron bands, as discussed in detail in Ref. [41], where

$$\Delta\chi''(\Omega) = \left(\frac{2}{\Omega}\right)^2 \text{Im} \left\{ \frac{\langle \gamma(\mathbf{k})g(\mathbf{k})\Delta_{e1}(\mathbf{k})\bar{P}(\tilde{\Omega}_{\mathbf{k}}) \rangle^2}{(\lambda_d^{-1} - \lambda_s^{-1}) - \langle g^2\bar{P}(\tilde{\Omega}_{\mathbf{k}}) \rangle} \right\}. \quad (6)$$

$\bar{P}(\tilde{\Omega}_{\mathbf{k}})$  is the response kernel with  $\tilde{\Omega}_{\mathbf{k}} = \Omega/[2\Delta_{e1}(\mathbf{k})]$ , such that

$$\bar{P}(\tilde{\Omega}_{\mathbf{k}}) = \begin{cases} \frac{\tilde{\Omega}_{\mathbf{k}}}{\sqrt{1-\tilde{\Omega}_{\mathbf{k}}^2}} \sin^{-1}(\tilde{\Omega}_{\mathbf{k}}) & |\tilde{\Omega}_{\mathbf{k}}| < 1 \\ \frac{\tilde{\Omega}_{\mathbf{k}}}{\sqrt{\tilde{\Omega}_{\mathbf{k}}^2-1}} \left[ \ln(|\tilde{\Omega}_{\mathbf{k}}| - \sqrt{\tilde{\Omega}_{\mathbf{k}}^2-1}) + i\frac{\pi}{2} \right] & |\tilde{\Omega}_{\mathbf{k}}| > 1 \end{cases} \quad (7)$$

(see Eq. (12) of Ref. [41] or, for isotropic systems, Eqs. (B6a)–(B6c) in Ref. [33]) and  $\lambda_s$  is the average coupling in the dominant  $s$ -wave ground state. The subdominant coupling  $\lambda_d$  is expressed as a fraction of  $\lambda_s$ . Note that the vertex  $\gamma(\mathbf{k})$  appears only linearly inside the Fermi-surface

average  $\langle \dots \rangle$ , implying that the sign of  $\gamma(\mathbf{k})$  becomes important. Equation (6) describes the BS pole inside the gap.

#### IV. RESULTS AND DISCUSSION

Figure 3 shows the comparison of experimental data and model calculations. The raw data [40] on which the spectra shown for Fig. 3 are based are a superposition of the electronic continuum and phonons. If the spectra measured right above  $T_c$  are subtracted from those in the superconducting state, only superconductivity-induced features survive. If the phonons are not sensitive to the superconducting transition, they disappear completely since the normal-state temperature dependence is already too weak to be visible below 50 K. In the case of the FeSCs, most of the phonons are indeed weakly coupled to the conduction electrons [62,63] and disappear after the subtraction. Only the  $B_{1g}$  Fe mode with an energy close to the gap edge becomes more intense, having some weak but finite coupling to the electronic states close to  $E_F$  and experiencing the increased density of states below  $T_c$ . However, the effect is much smaller than in A15 compounds [30], which possess a strong electron-phonon coupling, as an example. The continuum at energies above twice the gap maximum consists only of superconductivity-induced changes and vanishes at high energies, thus simplifying the comparison with weak-coupling results. In the gap region, the superconducting spectra have a smaller intensity than those for  $T > T_c$ , leading to negative difference spectra as an artifact of the subtraction procedure. In contrast, the fitted results also shown in Fig. 3 yield a vanishing intensity below the minimum gap energy. If the gap parameter approaches 0, such as in the normal state, the intensity vanishes completely in weak-coupling theory, making it inapplicable for describing the normal state or finite temperatures. Improvement could be achieved only by including all interactions, in particular, magnetism, in a realistic strong-coupling description of the FeSCs, which, however, is beyond the scope of this study.

All three symmetries show depletion of spectral weight in the low-energy region and an enhancement for energies larger than about  $160 \text{ cm}^{-1}$ . This behavior clearly indicates

TABLE I. Gap energies (meV) as obtained by Raman scattering and the present analysis compared to those from ARPES (Ref. [61]). The bands  $h1$ – $e2$  are color coded in Fig. 5 in Appendix A. Bands  $h1$  and  $h2$  cannot be distinguished in the ARPES experiment and therefore have the same entry.

| Band | $\Delta_{\text{min}}^{\text{Raman}}$ | $\Delta_{\text{max}}^{\text{Raman}}$ | $\Delta_{\text{av}}^{\text{ARPES}}$ |
|------|--------------------------------------|--------------------------------------|-------------------------------------|
| $h1$ | 9.5                                  | 12.1                                 | $12.3 \pm 0.6$                      |
| $h2$ | 10.4                                 | 15.9                                 | $12.3 \pm 0.6$                      |
| $h3$ | 4.2                                  | 5.0                                  | $5.8 \pm 0.8$                       |
| $e1$ | 10.3                                 | 13.3                                 | $12.2 \pm 0.3$                      |
| $e2$ | 10.8                                 | 11.4                                 | $11.4 \pm 0.5$                      |

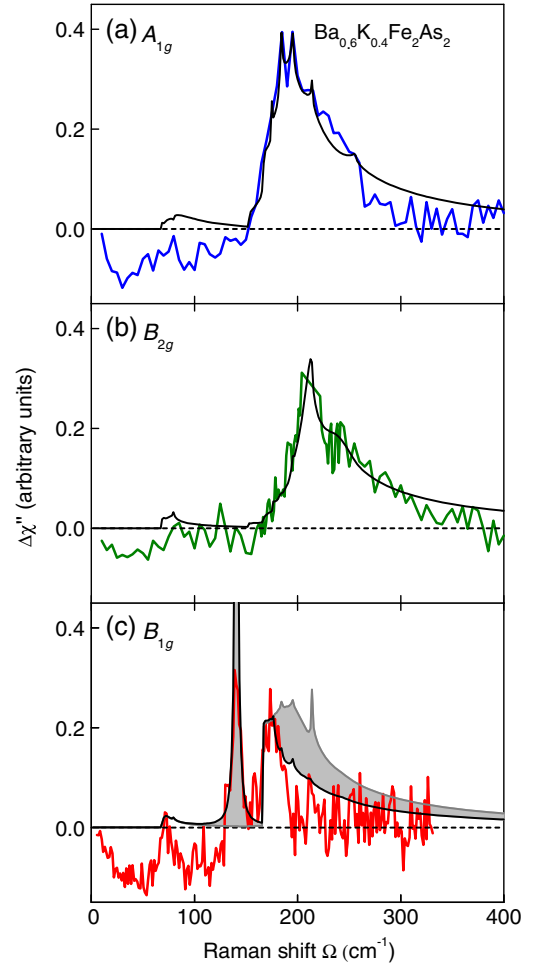


FIG. 3. Raman response and theoretical results for (a)  $A_{1g}$ , (b)  $B_{2g}$ , and (c)  $B_{1g}$  symmetry in  $\text{Ba}_{0.6}\text{K}_{0.4}\text{Fe}_2\text{As}_2$ . Shown is the difference  $\Delta\chi''$  of the response at 8 and 45 K (for raw data, see Ref. [40]). In this way, temperature-independent phonon lines and the particle-hole continuum are subtracted out, not being described by the weak-coupling theory. As an undesired side effect, the experimental intensities become negative inside the gap while the theoretical spectra just vanish. The sum of contributions from all bands is shown in black. Figure 5 of Appendix A shows a breakdown of contributions from individual bands. (c) The gray shaded area is the spectral weight transferred from the pair-breaking region into the collective mode.

the existence of a superconducting gap. Another common feature is a small enhancement at about  $70 \text{ cm}^{-1}$ . However, the sharp peak at  $140 \text{ cm}^{-1}$  in the  $B_{1g}$  channel, which is almost resolution limited, does not have a correspondence in the other symmetries and can be identified as a  $d$ -wave collective mode. The following discussion of the quantitative analysis is designed to support this interpretation and to reveal properties of both the superconducting gaps and the collective mode. The analysis is performed in two steps: (i) The momentum-dependent gaps on the various Fermi surfaces  $\Delta_n(\mathbf{k})$  are derived via an iterative process, and (ii) interactions are taken into account in the final state.

In the first step, only the  $A_{1g}$  and  $B_{2g}$  spectra are used, as described in detail in Appendix A. As a starting point, the gaps from angle-resolved photoemission spectroscopy (ARPES) (Ref. [61]) are used and refined such that well-defined momentum dependences along the  $k_z$  direction ( $-\pi < k_z < \pi$ ) are introduced for the gaps on the hole bands and within the  $k_x$ - $k_y$  plane for the gaps on the electron bands. Functionally, the gaps on the hole bands take the form  $\bar{\Delta}_n + \eta_n \cos(k_z)$  and those on the electron bands take the form  $\bar{\Delta}_n + \eta_n \cos(4\varphi)$ , where  $\varphi$ , the azimuthal angle as defined in Fig. 4, varies between 0 and  $2\pi$ . The values of all gaps derived from Raman and ARPES experiments are compiled in Table I with  $\bar{\Delta}_n = 1/2(\Delta_{\max,n}^{\text{Raman}} + \Delta_{\min,n}^{\text{Raman}})$  and  $\eta_n = 1/2(\Delta_{\max,n}^{\text{Raman}} - \Delta_{\min,n}^{\text{Raman}})$ .

Figure 4 shows false-color plots of the gap magnitudes in the 1 Fe reference frame that lead to the best agreement between Raman experiment and theory. The black lines in Fig. 3 show the total contribution of all  $n$  bands to the Raman spectra. We do not claim that the result is the only possible solution but we are convinced that there is little room for improvement, given the agreement between ARPES and all symmetries in the Raman scattering. The gap is as large as  $\Delta_{h2} = 15.9$  meV on the middle hole band ( $h2$ ) at  $k_z = 0$ . The minimal gap  $\Delta_{h3} = 4.2$  meV is found on the outer hole band ( $h3$ ). There are no nodes.

As opposed to the  $A_{1g}$  and the  $B_{2g}$  spectra, the  $B_{1g}$  spectrum cannot be reproduced with the choice of gaps summarized in Table I and Fig. 4. According to the Raman vertices, only the outer electron band  $e1$  contributes significantly while the intensity should be comparable in both the  $B_{2g}$  and  $B_{1g}$  symmetries. To resolve this discrepancy, the effect of an excitonic collective mode is introduced as a second step considering only the lowest-order ( $L = 2$ ) channel.

The subdominant coupling  $g$  shifts spectral weight from the pair-breaking peak into the sharp collective mode.

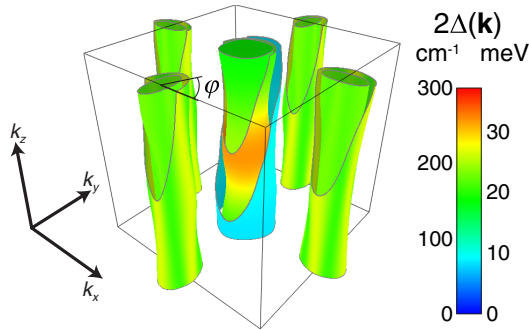


FIG. 4. Magnitudes (shown in false color) of the band-dependent gaps  $2\Delta_n(\mathbf{k})$  at the Fermi momentum  $\mathbf{k}_F$ . A moderate gap anisotropy is found on the middle hole band  $h2$  with the absolute gap maximum at  $k_z = 0$ . The gaps on the electron bands vary with the azimuthal angle  $\varphi$  and have maxima along the  $k_x$  and  $k_y$  axes. The gap anisotropies on the inner ( $h1$ ) and outer ( $h3$ ) hole bands and on the inner electron band ( $e2$ ) are negligible.

A momentum-dependent  $g(\mathbf{k})$  must be utilized, which reduces the response only at the gap maximum (rather than the minimum) while leading to the excitonic peak at  $140 \text{ cm}^{-1}$ . The best choice is a  $d$ -wave form for  $g(\mathbf{k})$ , which is small along diagonal directions to maximize the coupling between the gap maxima of the outer electron bands and, in addition, is proportional to the  $B_{1g}$  vertex [Eq. (2)]. The latter specialization is necessary since the linear  $B_{1g}$  vertex in Eq. (6) has several sign changes [see Fig. 2(c)] and would nearly cancel the weight of the collective mode for a weakly  $k$ -dependent  $g$ . This artifact originates in the fine structure of the  $B_{1g}$  vertex, which enters to lowest order quadratically, but linearly in the vertex. The choice of  $g(\mathbf{k}) \propto \gamma^{B_{1g}}(\mathbf{k})$  is physically justified and ensures that the spectral weights of both the bare bubble and the vertex correction come from the same parts of the Fermi surface. This argument is particularly relevant for comparing the two coupling channels.

In fact, the transfer of spectral weight encodes the relative strength between the  $s$  and  $d$  channels. In addition to the weight transfer, the position of the collective mode depends on  $(\lambda_d/\lambda_s)^2$  as derived for an isotropic gap by Monien and Zawadowski [33]. With the maximal gap  $2\Delta_{\max}$  of  $210 \text{ cm}^{-1}$  on the  $e1$  band and the collective mode at  $140 \text{ cm}^{-1}$ , the binding energy is as large as one third of  $2\Delta_{\max}$ , yielding  $\lambda_d \approx 0.6\lambda_s$ . A similar ratio was used in the model calculations of Ref. [41]. The related transfer of approximately one half of the spectral weight from the pair-breaking maximum into the bound state (Fig. 3) is consistent with the energy shift.

This rather high fraction highlights that the subdominant  $d$ -wave channel lies in close proximity to the  $s$ -wave channel, such that if the  $s$ -wave channel weakens, for instance, as a result of a change of the Fermi surface, a new dominant symmetry emerges and a BS mode would flip identity as a subdominant  $s$ -wave bound-state exciton. We speculate that a dominant  $d$ -wave coupling could be realized in FeSe (Refs. [17,64]) and alkali-doped selenides such as  $\text{Rb}_{0.8}\text{Fe}_{1.6}\text{Se}_2$ , although the pairing symmetry in these systems is still a matter of intense discussion [10,40,65–68].

## V. CONCLUSIONS

We studied the temperature dependence of the  $B_{1g}$  Raman spectra in  $\text{Ba}_{0.6}\text{K}_{0.4}\text{Fe}_2\text{As}_2$  and proposed a realistic model calculation for the superconducting response at low temperatures that reproduces the spectra almost quantitatively. The temperature dependence observed for the prominent peaks and the theoretical analysis demonstrate that only the  $B_{1g}$  mode at  $140 \text{ cm}^{-1}$  has all features expected for the elusive BS mode in the presence of competing pairing symmetries: (i) It lies below twice the gap edge, (ii) has an almost resolution-limited width, (iii) has a temperature dependence that is dominated by that of the single-particle gap, and (iv) drains spectral

weight from the pair-breaking peaks. The BS mode results from higher-order (vertex) corrections that render the theory gauge invariant but are usually considered physically unimportant. Here, they prove to be instrumental to pin down the hierarchy of superconducting channels. In particular, we find that the coupling parameter in the subdominant  $d_{x^2-y^2}$  channel reaches 60% of the prevailing  $s$ -wave pairing state, making  $d_{x^2-y^2}$  pairing a candidate for materials without central hole bands.

The  $d_{x^2-y^2}$  channel competes with the  $s$  ground state (independent of whether it is  $s_{+-}$  or  $s_{++}$  being indistinguishable by spectroscopy) since the gaps on electron bands have the same sign whereas the  $d_{x^2-y^2}$  channel would lead to a phase difference of  $\pi$  between neighboring electron bands. Although the  $d$  channel is already quite strong in  $\text{Ba}_{0.6}\text{K}_{0.4}\text{Fe}_2\text{As}_2$ , the gaps on the various Fermi surfaces are not yet very anisotropic. For this reason,  $T_c$  is relatively high, and the density of states between the large and the small gaps is sufficiently small on the relevant bands, thus keeping the damping of the excitonic mode small. If the ratio of the coupling strengths comes closer to 1, the frustration between the  $s$  and  $d$  channels increases, the gaps become more anisotropic [5], and consequently,  $T_c$  decreases. An existing BS mode would then be damped strongly and hardly visible. This scenario could, in fact, apply for  $\text{Ba}(\text{Fe}_{1-x}\text{Co}_x)_2\text{As}_2$ .

If, on the other hand, the central hole bands disappear, such as in  $\text{Rb}_{0.8}\text{Fe}_{1.6}\text{Se}_2$  or appropriately annealed  $\text{FeSe}$  [6], the  $d$  channel would prevail and could establish nodeless  $d_{x^2-y^2}$  pairing. Since the gap is then quasi-isotropic,  $T_c$  can be comparably high as in the  $s$  channel. From this point of view, the transition temperatures in the cuprates are not yet maximal since the gap has nodes on the Fermi surface. In any case, Raman scattering directly shows the symmetry of the competing pairing channels in  $\text{Ba}_{0.6}\text{K}_{0.4}\text{Fe}_2\text{As}_2$  and thus supports (i) the dominance of electronically driven pairing and (ii) points toward directions for engineering of higher transition temperatures.

### ACKNOWLEDGMENTS

We acknowledge useful discussions with Ming Yi. The work was supported by the DFG via the Priority Program SPP 1458 (Project No. HA 2071/7) and, partially, via the Transregional Collaborative Research Center TRR 80. Additional support came from the Bavarian Californian Technology Center BaCaTeC (Project No. A5). R. H. thanks the Stanford Institute for Materials and Energy Sciences (SIMES) at Stanford University and SLAC National Accelerator Laboratory for hospitality. Work in the SIMES at Stanford and SLAC was supported by the U.S. Department of Energy, Office of Basic Energy Sciences, Division of Materials Sciences and Engineering, under Contract No. DE-AC02-76SF00515.

### APPENDIX A: BAND-RESOLVED CONTRIBUTIONS TO THE SCATTERING

An ideal starting point for the analysis of the band and momentum dependences of the gaps in  $\text{Ba}_{0.6}\text{K}_{0.4}\text{Fe}_2\text{As}_2$  is the  $B_{2g}$  spectrum, which is free of collective modes and screening effects. Equation (5) can be applied separately for each band with additive results. In Fig. 5, the contributions from the five bands  $h1$ – $e2$  crossing  $E_F$  are plotted. The Fermi surfaces are shown schematically in the inset with the colors corresponding to those of the theoretical spectra. One finds that only the contributions from the outer electron band ( $e1$ , light blue line in Fig. 5) and the middle hole band ( $h2$ , red line) are large enough to contribute significantly to the response above  $160\text{ cm}^{-1}$ , with the contribution from the outer electron band approximately twice as large as that of the middle hole band. This

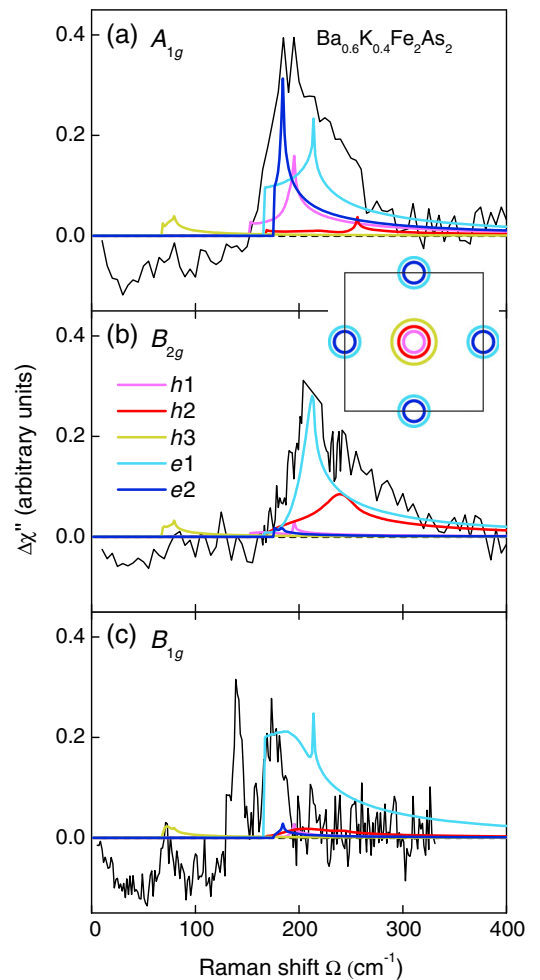


FIG. 5. Contributions of the different bands to the cross section. Shown are the individual contributions of the five bands  $h1$ – $e2$ , as indicated in (b), to the total cross section, as displayed in Fig. 3, for (a)  $A_{1g}$ , (b)  $B_{2g}$ , and (c)  $B_{1g}$  symmetry. The inset shows a sketch of the first BZ with the corresponding color code for the Fermi surfaces. The experimental data are shown in black.

difference can be anticipated just by looking at the  $B_{2g}$  Raman vertices of Fig. 2 with a high intensity on the outer electron band, a smaller intensity for the middle hole band, and vanishingly small intensities from the other bands. To reproduce fully the increase of the spectrum between  $160 \text{ cm}^{-1}$  and the maximum at  $210 \text{ cm}^{-1}$ , it is necessary to (i) adjust the minimum and maximum gap values on band  $e1$  and (ii) align the gap minimum with the minimum of the Raman vertex. This alignment allows one to reproduce the experimental slope without a spectral discontinuity. For band  $e1$ , one assumes that the gap has fourfold symmetry, with the maxima aligned along the  $k_x$  and  $k_y$  axes, and with no  $k_z$  dispersion for the fit. The remaining shoulder on the high-energy side of the peak can be reproduced with a  $k_z$  dispersive gap on the middle hole band having the maximum and the minimum at  $k_z = 0$  and  $k_z = \pm\pi$ , respectively. The gap maxima and minima are given in Table I. The functional variations along  $k_z$  and in the basal plane are in the main text. The black line in Fig. 3(b) is the sum of all contributions.

For the  $A_{1g}$  spectrum, the inner hole band ( $h1$ , magenta line) and the inner electron band ( $e2$ , dark blue line) become important [Fig. 5(a)]. However, neither band can be expected to produce a feature at  $70 \text{ cm}^{-1}$  because the contributions from  $h1$  and  $e2$  would be too large in  $A_{1g}$  symmetry but too small in the  $B_{1g}$  spectrum. Hence, the outer hole band ( $h3$ , light green line), for which the nesting condition is worse than for the other bands, is used to reproduce the feature at  $70 \text{ cm}^{-1}$ . The two remaining bands  $h2$  and  $e1$  are used to reproduce the shape in the  $190 \text{ cm}^{-1}$  range, being approximately  $20 \text{ cm}^{-1}$  below the maximum in  $B_{2g}$  symmetry. The black line in Fig. 3(a) is the sum of all contributions.

The  $B_{1g}$  spectra cannot be described on the basis of the gaps derived from the  $A_{1g}$  and  $B_{2g}$  spectra, as shown by the gray line in Fig. 3(c) representing the sum of all bands without final-state interaction. Since the  $B_{1g}$  spectra approach 0 already above  $200 \text{ cm}^{-1}$ , there is no way to achieve better agreement between theory and experiment in the lowest order [see Eq. (5)]. Only in the presence of final-state interactions [see Eq. (6)] are the spectra above  $200 \text{ cm}^{-1}$  depleted and do they approach the experimental result, as described in the text. The black line in Fig. 3(c) represents the full theoretical result.

## APPENDIX B: INFLUENCE OF THE BACKFOLDING

The simplest elementary cell has just one Fe atom per quadratic unit cell. This choice is motivated by the low-energy band structure of the FeSCs being derived only from Fe  $3d$  orbitals. The resulting five bands reproduce the Fermi surfaces qualitatively, but the magnetism cannot be treated appropriately. From the viewpoint of light scattering, the 1 Fe cell proves sufficient for a qualitative understanding of the selection rules [48]. However, the backfolding due to

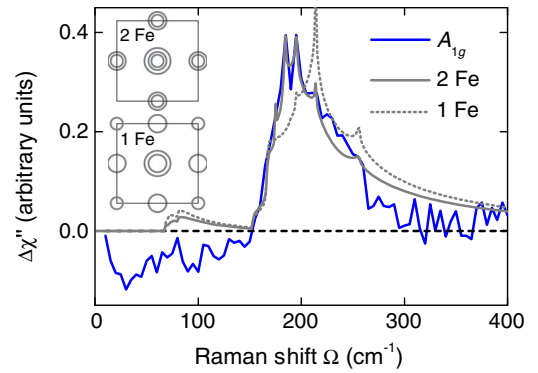


FIG. 6. Results for  $A_{1g}$  symmetry for (a) 1 Fe and (b) 2 Fe zone vertices. The gap parameters are unchanged. The insets show the bands for both cases. The difference between the  $A_{1g}$  spectra is the biggest one of all symmetries.

the inclusion of the As atoms and  $\text{BaFe}_2\text{As}_2$ , having a body-centered-tetragonal unit cell, changes the band structure considerably and also influences the selection rules [52]. In addition, the backfolding changes the spectral weight on the bands [69], further complicating the evaluation of one- and two-particle response functions.

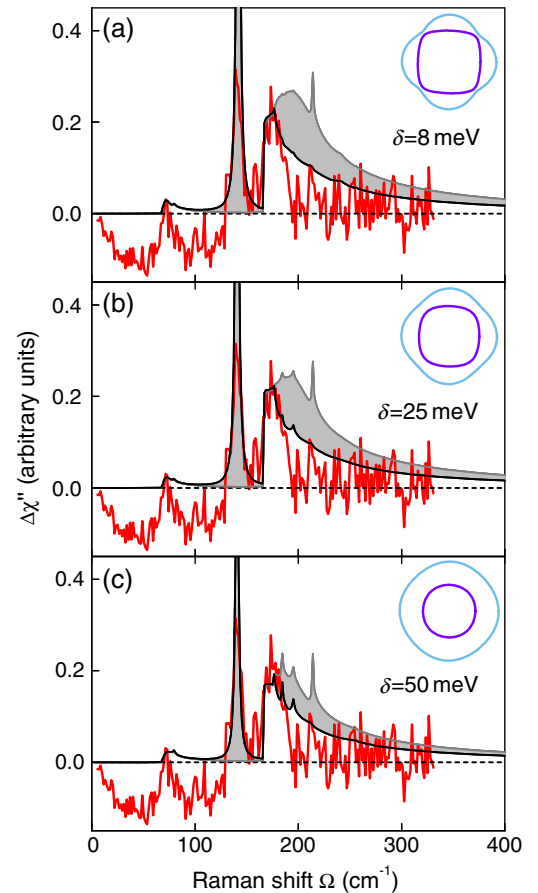


FIG. 7. Results for  $B_{1g}$  symmetry using different hybridization energies  $\delta$  as indicated. The insets show a cut through the two electron bands at  $k_z = \pi/2$ .

In our study, we found good agreement upon using the band structure of the 2 Fe unit cell. In addition to these calculations, we redid some of the calculations in the 1 Fe cell. In Fig. 6, we show the results for  $A_{1g}$  symmetry. While the overall shape is conserved, there are minor but significant differences around the gap maximum. Therefore, if numerical studies are performed, the 2 Fe cell is preferable although the symmetry assignment is better done in the 1 Fe cell, since otherwise, the generic meaning of the respective symmetries becomes compromised. For instance, the  $x^2 - y^2$  symmetry being projected in the  $B_{1g}$  spectra is the proper symmetry for both nematic fluctuations and the subdominant  $d$  pairing channel discussed here. In the 2 Fe cell, one would have to switch to the  $B_{2g}$  or  $xy$  channel, which appears awkward.

The backfolding makes the electron bands overlap. Since the electrons belong to the same orbitals, the bands hybridize at the intersection points. As was shown by Mazin and co-workers [52] and by Eiter *et al.* [70], the cross section may be enhanced substantially at the hybridization point from the resulting increased band curvature and the spectra may change accordingly. Therefore, we also studied the effect of hybridization by calculating the  $B_{1g}$  Raman spectra for various hybridization energies  $\delta$  and plot the results in Fig. 7.  $B_{1g}$  is the most important symmetry in this context since the electron bands are the battleground of the  $s_{+-}$  and  $d_{x^2-y^2}$  pairing channels. Although the Fermi-surface shape clearly changes, the spectra show only minor differences since the integrated spectral weight around the hybridization lines is almost independent of  $\delta$ , as opposed to the results for  $\text{Ba}(\text{Fe}_{1-x}\text{Co}_x)_2\text{As}_2$  (Ref. [52]). We conclude that the influence of the hybridization does not complicate our argumentation. Rather, the results are robust and show only small quantitative differences for the 1 Fe and 2 Fe bases.

---

[1] I. I. Mazin, D. J. Singh, M. D. Johannes, and M. H. Du, *Unconventional Superconductivity with a Sign Reversal in the Order Parameter of  $\text{LaFeAsO}_{1-x}\text{F}_x$* , *Phys. Rev. Lett.* **101**, 057003 (2008).  
 [2] R. M. Fernandes and A. J. Millis, *Suppression of Superconductivity by Néel-Type Magnetic Fluctuations in the Iron Pnictides*, *Phys. Rev. Lett.* **110**, 117004 (2013).  
 [3] S. Liang, A. Moreo, and E. Dagotto, *Nematic State of Pnictides Stabilized by Interplay between Spin, Orbital, and Lattice Degrees of Freedom*, *Phys. Rev. Lett.* **111**, 047004 (2013).  
 [4] A. F. Kemper, T. A. Maier, S. Graser, H.-P. Cheng, P. J. Hirschfeld, and D. J. Scalapino, *Sensitivity of the Superconducting State and Magnetic Susceptibility to Key Aspects of Electronic Structure in Ferropnictides*, *New J. Phys.* **12**, 073030 (2010).

[5] P. J. Hirschfeld, M. M. Korshunov, and I. I. Mazin, *Gap Symmetry and Structure of Fe-Based Superconductors*, *Rep. Prog. Phys.* **74**, 124508 (2011).  
 [6] S. He *et al.*, *Phase Diagram and Electronic Indication of High-Temperature Superconductivity at 65 K in Single-Layer  $\text{FeSe}$  Films*, *Nat. Mater.* **12**, 605 (2013).  
 [7] J. J. Lee, F. T. Schmitt, R. G. Moore, S. Johnston, Y.-T. Cui, W. Li, M. Yi, Z. K. Liu, M. Hashimoto, Y. Zhang, D. H. Lu, T. P. Devereaux, D.-H. Lee, and Z.-X. Shen, *Significant  $T_c$  Enhancement in  $\text{FeSe}$  Films on  $\text{SrTiO}_3$  due to Anomalous Interfacial Mode Coupling*, arXiv:1312.2633.  
 [8] R. Thomale, C. Platt, J. Hu, C. Honerkamp, and B. Andrei Bernevig, *Functional Renormalization-Group Study of the Doping Dependence of Pairing Symmetry in the Iron Pnictide Superconductors*, *Phys. Rev. B* **80**, 180505 (2009).  
 [9] R. Thomale, C. Platt, W. Hanke, and B. Andrei Bernevig, *Mechanism for Explaining Differences in the Order Parameters of FeAs-Based and FeP-Based Pnictide Superconductors*, *Phys. Rev. Lett.* **106**, 187003 (2011).  
 [10] L. Sun, X.-J. Chen, J. Guo, P. Gao, Q.-Z. Huang, H. Wang, M. Fang, X. Chen, G. Chen, Q. Wu, C. Zhang, D. Gu, X. Dong, L. Wang, K. Yang, A. Li, X. Dai, H.-k. Mao, and Z. Zhao, *Re-emerging Superconductivity at 48 Kelvin in Iron Chalcogenides*, *Nature (London)* **483**, 67 (2012).  
 [11] F. F. Tafti, A. Juneau-Fecteau, M.-È. Delange, S. René de Cotret, J.-Ph. Reid, A. F. Wang, X.-G. Luo, X. H. Chen, N. Doiron-Leyraud, and L. Taillefer, *Sudden Reversal in the Pressure Dependence of  $T_c$  in the Iron-Based Superconductor  $\text{KFe}_2\text{As}_2$* , *Nat. Phys.* **9**, 349 (2013).  
 [12] F. F. Tafti, J. P. Clancy, M. Lapointe-Major, C. Collignon, S. Faucher, J. A. Sears, A. Juneau-Fecteau, N. Doiron-Leyraud, A. F. Wang, X.-G. Luo, X. H. Chen, S. Desgreniers, Y.-J. Kim, and L. Taillefer, *Sudden Reversal in the Pressure Dependence of  $T_c$  in the Iron-Based Superconductor  $\text{CsFe}_2\text{As}_2$ : A Possible Link between Inelastic Scattering and Pairing Symmetry*, *Phys. Rev. B* **89**, 134502 (2014).  
 [13] A. D. Christianson, E. A. Goremychkin, R. Osborn, S. Rosenkranz, M. D. Lumsden, C. D. Malliakas, I. S. Todorov, H. Claus, D. Y. Chung, M. G. Kanatzidis, R. I. Bewley, and T. Guidi, *Unconventional Superconductivity in  $\text{Ba}_{0.6}\text{K}_{0.4}\text{Fe}_2\text{As}_2$  from Inelastic Neutron Scattering*, *Nature (London)* **456**, 930 (2008).  
 [14] H. Kontani and S. Onari, *Orbital-Fluctuation-Mediated Superconductivity in Iron Pnictides: Analysis of the Five-Orbital Hubbard-Holstein Model*, *Phys. Rev. Lett.* **104**, 157001 (2010).  
 [15] S. Graser, T. A. Maier, P. J. Hirschfeld, and D. J. Scalapino, *Near-Degeneracy of Several Pairing Channels in Multi-orbital Models for the Fe Pnictides*, *New J. Phys.* **11**, 025016 (2009).  
 [16] S. Graser, A. F. Kemper, T. A. Maier, H.-P. Cheng, P. J. Hirschfeld, and D. J. Scalapino, *Spin Fluctuations and Superconductivity in a Three-Dimensional Tight-Binding Model for  $\text{BaFe}_2\text{As}_2$* , *Phys. Rev. B* **81**, 214503 (2010).  
 [17] T. Hanaguri, S. Niitaka, K. Kuroki, and H. Takagi, *Unconventional  $s$ -Wave Superconductivity in  $\text{Fe}(\text{Se},\text{Te})$* , *Science* **328**, 474 (2010).  
 [18] T. P. Devereaux and R. Hackl, *Inelastic Light Scattering from Correlated Electrons*, *Rev. Mod. Phys.* **79**, 175 (2007).

- [19] A. J. Leggett, *Number-Phase Fluctuations in Two-Band Superconductors*, *Prog. Theor. Phys.* **36**, 901 (1966).
- [20] M. V. Klein, *Theory of Raman Scattering from Leggett's Collective Mode in a Multiband Superconductor: Application to MgB<sub>2</sub>*, *Phys. Rev. B* **82**, 014507 (2010).
- [21] G. Blumberg, A. Mialitsin, B. S. Dennis, M. V. Klein, N. D. Zhigadlo, and J. Karpinski, *Observation of Leggett's Collective Mode in a Multiband MgB<sub>2</sub> Superconductor*, *Phys. Rev. Lett.* **99**, 227002 (2007).
- [22] R. Sooryakumar and M. V. Klein, *Raman Scattering by Superconducting-Gap Excitations and Their Coupling to Charge-Density Waves*, *Phys. Rev. Lett.* **45**, 660 (1980).
- [23] P. B. Littlewood and C. M. Varma, *Gauge-Invariant Theory of the Dynamical Interaction of Charge Density Waves and Superconductivity*, *Phys. Rev. Lett.* **47**, 811 (1981).
- [24] I. Tüttő and A. Zawadowski, *Theory of Raman Scattering of Superconducting Amplitude Modes in Charge-Density-Wave Superconductors*, *Phys. Rev. B* **45**, 4842 (1992).
- [25] C. M. Varma, *Higgs Boson in Superconductors*, *J. Low Temp. Phys.* **126**, 901 (2002).
- [26] Y. Barlas and C. M. Varma, *Amplitude or Higgs Modes in d-Wave Superconductors*, *Phys. Rev. B* **87**, 054503 (2013).
- [27] D. Einzel (private communication).
- [28] P. B. Littlewood and C. M. Varma, *Amplitude Collective Modes in Superconductors and Their Coupling to Charge-Density Waves*, *Phys. Rev. B* **26**, 4883 (1982).
- [29] R. Hackl, R. Kaiser, and S. Schickanz, *Gap Mode, Superconducting Gap and Phonon Mode in V<sub>3</sub>Si and Nb<sub>3</sub>Sn*, *J. Phys. C* **16**, 1729 (1983).
- [30] R. Hackl, R. Kaiser, and W. Gläser, *Electronic and Phonon-Mediated Gap Modes in A15 Compounds*, *Physica (Amsterdam)* **162C–164C**, 431 (1989).
- [31] M.-A. Méasson, Y. Gallais, M. Cazayous, B. Clair, P. Rodière, L. Cario, and A. Sacuto, *Amplitude Higgs Mode in the 2H-NbSe<sub>2</sub> Superconductor*, *Phys. Rev. B* **89**, 060503 (2014).
- [32] W. Rehwald, M. Rayl, R. W. Cohen, and G. D. Cody, *Elastic Moduli and Magnetic Susceptibility of Monocrystalline Nb<sub>3</sub>Sn*, *Phys. Rev. B* **6**, 363 (1972).
- [33] H. Monien and A. Zawadowski, *Theory of Raman Scattering with Final-State Interaction in High-T<sub>c</sub> BCS Superconductors: Collective Modes*, *Phys. Rev. B* **41**, 8798 (1990).
- [34] A. Bardasis and J. R. Schrieffer, *Excitons and Plasmons in Superconductors*, *Phys. Rev.* **121**, 1050 (1961).
- [35] M. V. Klein and S. B. Dierker, *Theory of Raman Scattering in Superconductors*, *Phys. Rev. B* **29**, 4976 (1984).
- [36] A. V. Chubukov, I. Eremin, and M. M. Korshunov, *Theory of Raman Response of a Superconductor with Extended s-Wave Symmetry: Application to the Iron Pnictides*, *Phys. Rev. B* **79**, 220501 (2009).
- [37] T. P. Devereaux and D. Einzel, *Electronic Raman Scattering in Superconductors as a Probe of Anisotropic Electron Pairing*, *Phys. Rev. B* **51**, 16336 (1995).
- [38] T. J. Greytak and J. Yan, *Light Scattering from Rotons in Liquid Helium*, *Phys. Rev. Lett.* **22**, 987 (1969).
- [39] A. Zawadowski, J. Ruvalds, and J. Solana, *Bound Roton Pairs in Superfluid Helium*, *Phys. Rev. A* **5**, 399 (1972).
- [40] F. Kretzschmar, B. Muschler, T. Böhm, A. Baum, R. Hackl, H.-H. Wen, V. Tsurkan, J. Deisenhofer, and A. Loidl, *Raman-Scattering Detection of Nearly Degenerate s-Wave and d-Wave Pairing Channels in Iron-Based Ba<sub>0.6</sub>K<sub>0.4</sub>Fe<sub>2</sub>As<sub>2</sub> and Rb<sub>0.8</sub>Fe<sub>1.6</sub>As<sub>2</sub> Superconductors*, *Phys. Rev. Lett.* **110**, 187002 (2013).
- [41] D. J. Scalapino and T. P. Devereaux, *Collective d-Wave Exciton Modes in the Calculated Raman Spectrum of Fe-Based Superconductors*, *Phys. Rev. B* **80**, 140512 (2009).
- [42] W.-C. Lee, S.-C. Zhang, and C. Wu, *Pairing State with a Time-Reversal Symmetry Breaking in FeAs-Based Superconductors*, *Phys. Rev. Lett.* **102**, 217002 (2009).
- [43] W.-C. Lee and P. W. Phillips, *Orbital Resonance Mode in Superconducting Iron Pnictides*, *Europhys. Lett.* **103**, 57003 (2013).
- [44] T. P. Devereaux, *Theory for the Effects of Impurities on the Raman Spectra of Superconductors*, *Phys. Rev. B* **45**, 12965 (1992).
- [45] T. P. Devereaux, *Theory for the Effects of Impurities on the Raman Spectra of Superconductors. II. Temperature Dependence and Influence of Final-State Interactions*, *Phys. Rev. B* **47**, 5230 (1993).
- [46] D. Manske, *Theory of Unconventional Superconductors*, Springer Tracts in Modern Physics Vol. 202 (Springer, New York, 2004).
- [47] D. V. Evtushinsky, D. S. Inosov, V. B. Zabolotnyy, A. Koitzsch, M. Knupfer, B. Buchner, M. S. Viazovska, G. L. Sun, V. Hinkov, A. V. Boris, C. T. Lin, B. Keimer, A. Varykhalov, A. A. Kordyuk, and S. V. Borisenko, *Momentum Dependence of the Superconducting Gap in Ba<sub>1-x</sub>K<sub>x</sub>Fe<sub>2</sub>As<sub>2</sub>*, *Phys. Rev. B* **79**, 054517 (2009).
- [48] B. Muschler, W. Prestel, R. Hackl, T. P. Devereaux, J. G. Analytis, J.-H. Chu, and I. R. Fisher, *Band- and Momentum-Dependent Electron Dynamics in Superconducting Ba(Fe<sub>1-x</sub>Co<sub>x</sub>)<sub>2</sub>As<sub>2</sub> as Seen via Electronic Raman Scattering*, *Phys. Rev. B* **80**, 180510 (2009).
- [49] The A<sub>2g</sub> component is generally weak in FeSCs. In Ba<sub>0.6</sub>K<sub>0.4</sub>Fe<sub>2</sub>As<sub>2</sub>, the full symmetry analysis is performed only at 200 K, and the overall intensity of all other symmetries is at least a factor of 2 stronger than in A<sub>2g</sub> symmetry.
- [50] What we call background here is the particle-hole continuum containing information on the electron dynamics [18] that can be extracted in a similar way as from the optical conductivity [51]. Since we do not have a microscopic model, we use a smooth analytic function to approximate it, so as to extract reliably the peak frequencies of the pair-breaking maximum and the BS mode.
- [51] M. Opel, R. Nemetschek, C. Hoffmann, R. Philipp, P. F. Müller, R. Hackl, I. Tüttő, A. Erb, B. Revaz, E. Walker, H. Berger, and L. Forró, *Carrier Relaxation, Pseudogap, and Superconducting Gap in High-T<sub>c</sub> Cuprates: A Raman Scattering Study*, *Phys. Rev. B* **61**, 9752 (2000).
- [52] I. I. Mazin, T. P. Devereaux, J. G. Analytis, J.-H. Chu, I. R. Fisher, B. Muschler, and R. Hackl, *Pinpointing Gap Minima in Ba(Fe<sub>0.94</sub>Co<sub>0.06</sub>)<sub>2</sub>As<sub>2</sub> via Band-Structure Calculations and Electronic Raman Scattering*, *Phys. Rev. B* **82**, 180502 (2010).
- [53] T. P. Devereaux, D. Einzel, B. Stadlober, R. Hackl, D. H. Leach, and J. J. Neumeier, *Electronic Raman Scattering in*

- High- $T_c$  Superconductors: A Probe of  $d_{x^2-y^2}$  Pairing*, *Phys. Rev. Lett.* **72**, 396 (1994).
- [54] P. B. Allen, *Fermi-Surface Harmonics: A General Method for Nonspherical Problems. Application to Boltzmann and Eliashberg Equations*, *Phys. Rev. B* **13**, 1416 (1976).
- [55] W. Hayes and R. Loudon, *Scattering of Light by Crystals* (Dover, New York, 2005).
- [56] N. W. Ashcroft and N. D. Mermin, *Solid State Physics* (Saunders College, Philadelphia, 1976), p. 848.
- [57] L. Chauvière, Y. Gallais, M. Cazayous, M. A. Méasson, A. Sacuto, D. Colson, and A. Forget, *Impact of the Spin-Density-Wave Order on the Superconducting Gap of  $\text{Ba}(\text{Fe}_{1-x}\text{Co}_x)_2\text{As}_2$* , *Phys. Rev. B* **82**, 180521 (2010).
- [58] T. Tsuneto, *Transverse Collective Excitations in Superconductors and Electromagnetic Absorption*, *Phys. Rev.* **118**, 1029 (1960).
- [59] T. P. Devereaux, A. Virosztek, and A. Zawadowski, *Multiband Electronic Raman Scattering in Bilayer Superconductors*, *Phys. Rev. B* **54**, 12 523 (1996).
- [60] G. R. Boyd, T. P. Devereaux, P. J. Hirschfeld, V. Mishra, and D. J. Scalapino, *Probing the Pairing Symmetry of the Iron Pnictides with Electronic Raman Scattering*, *Phys. Rev. B* **79**, 174521 (2009).
- [61] K. Nakayama, T. Sato, P. Richard, Y.-M. Xu, Y. Sekiba, S. Souma, G. F. Chen, J. L. Luo, N. L. Wang, H. Ding, and T. Takahashi, *Superconducting Gap Symmetry of  $\text{Ba}_{0.6}\text{K}_{0.4}\text{Fe}_2\text{As}_2$  Studied by Angle-Resolved Photoemission Spectroscopy*, *Europhys. Lett.* **85**, 67 002 (2009).
- [62] L. Boeri, O. V. Dolgov, and A. A. Golubov, *Is  $\text{LaFeAsO}_{1-x}\text{F}_x$  an Electron-Phonon Superconductor?*, *Phys. Rev. Lett.* **101**, 026403 (2008).
- [63] M. Rahlenbeck, G. L. Sun, D. L. Sun, C. T. Lin, B. Keimer, and C. Ulrich, *Phonon Anomalies in Pure and Underdoped  $\text{R}_{1-x}\text{K}_x\text{Fe}_2\text{As}_2$  ( $\text{R} = \text{Ba}, \text{Sr}$ ) Investigated by Raman Light Scattering*, *Phys. Rev. B* **80**, 064509 (2009).
- [64] R. Yu, P. Goswami, Q. Si, P. Nikolic, and J.-X. Zhu, *Superconductivity at the Boarder of Electron Localization and Itineracy*, *Nat. Commun.* **4**, 2783 (2013).
- [65] T. Qian, X.-P. Wang, W.-C. Jin, P. Zhang, P. Richard, G. Xu, X. Dai, Z. Fang, J.-G. Guo, X.-L. Chen, and H. Ding, *Absence of a Holelike Fermi Surface for the Iron-Based  $\text{KFe}_{1.7}\text{Se}_2$  Superconductor Revealed by Angle-Resolved Photoemission Spectroscopy*, *Phys. Rev. Lett.* **106**, 187001 (2011).
- [66] I. I. Mazin, *Symmetry Analysis of Possible Superconducting States in  $\text{K}_x\text{Fe}_y\text{Se}_2$  Superconductors*, *Phys. Rev. B* **84**, 024529 (2011).
- [67] X.-P. Wang, P. Richard, X. Shi, A. Roeyghem, Y.-B. Huang, E. Razzoli, T. Qian, E. Rienks, S. Thirupathiah, H.-D. Wang, C.-H. Dong, M.-H. Fang, M. Shi, and H. Ding, *Observation of an Isotropic Superconducting Gap at the Brillouin Zone Centre of  $\text{Tl}_{0.63}\text{K}_{0.37}\text{Fe}_{1.78}\text{Se}_2$* , *Europhys. Lett.* **99**, 67 001 (2012).
- [68] M. Khodas and A. V. Chubukov, *Interpocket Pairing and Gap Symmetry in Fe-Based Superconductors with Only Electron Pockets*, *Phys. Rev. Lett.* **108**, 247003 (2012).
- [69] C.-H. Lin, T. Berlijn, L. Wang, C.-C. Lee, W.-G. Yin, and W. Ku, *One-Fe versus Two-Fe Brillouin Zone of Fe-Based Superconductors: Creation of the Electron Pockets by Translational Symmetry Breaking*, *Phys. Rev. Lett.* **107**, 257001 (2011).
- [70] H.-M. Eiter, M. Lavagnini, R. Hackl, E. A. Nowadnick, A. F. Kemper, T. P. Devereaux, J.-H. Chu, J. G. Analytis, I. R. Fisher, and L. Degiorgi, *Alternative Route to Charge Density Wave Formation in Multiband Systems*, *Proc. Natl. Acad. Sci. U.S.A.* **110**, 64 (2013).